Passive Metashells with Adaptive Thermal Conductivities: Chameleonlike Behavior and Its Origin

Liujun Xu, Shuai Yang, and Jiping Huang*

Department of Physics, State Key Laboratory of Surface Physics, and Key Laboratory of Micro and Nano Photonic Structures (MOE), Fudan University, Shanghai 200433, China

(Received 18 June 2018; revised manuscript received 15 March 2019; published 24 May 2019)

Chameleons have the ability to change their colors to adapt to nearby objects. Here, we introduce this behavior from optics to thermotics. By theory, simulation, and experiment, we design and fabricate a class of counterintuitive chameleonlike metashells: they exhibit adaptive thermal responses to changing objects in the vicinity (such objects are characterized by changing thermal conductivities and/or temperature distributions), even though their thermal conductivities are passive (without any preknowledge of the changing objects). We reveal the underlying mechanism by deriving the specific relations governing the components of tensorial conductivities of the metashells. Our metashells are passive, but they display adaptivity, which can work as a type of all-purpose material to meet different requirements of thermal conductivities under different conditions. The potential applications are to realize novel camouflaging, self-adaption, etc. This work gives a passive method for exploring intelligent thermal metamaterials in contrast to the existing active methods, and it also offers guidance for designing similar behaviors in electrostatics, magnetostatics, and particle diffusion.

DOI: 10.1103/PhysRevApplied.11.054071

I. INTRODUCTION

Thermal cloaks [1–11] have aroused intense interest for their potential application in protecting the objects inside from being detected. From the perspective of thermal conductivity, the most striking feature of thermal cloaks is the fixed overall effective thermal conductivity.

Nevertheless, these schemes are "active" because of the necessity of considering environmental effects in advance, rather than "passive," without the preknowledge of environments. Concretely speaking, when a traditional cloak (i.e., without external control) [1–8] is designed, the thermal conductivity of the cloak is related to that of the environment outside the cloak; when a nontraditional cloak (i.e., with external control) [9–11] is designed, the temperature distribution of the environment should be taken into consideration.

Therefore, in spite of the excellent performance of thermal cloaks, the fixed and active material properties may lack the feasibility to adapt to environmental changes. Owing to actual application requirements (such as all-purpose materials), it is urgent to explore thermal metamaterials that have adaptive responses to environments, which may be called "intelligent thermal metamaterials" hereafter.

In this direction, several papers have been published that take into account the temperature dependence of thermal conductivities [12–14] or permittivities [15]. However, the relevant methods are active (not passive), as defined above. For such methods, a severe limitation is that the environment plays a dominant role in designing and fabricating the intelligent metamaterials, which still restricts applications.

To overcome this limitation, here we propose a passive method, which allows us to achieve intelligent thermal metamaterials without the need to consider the influence of environments. As a result, we successfully design and fabricate a class of counterintuitive chameleonlike metashells whose effective thermal conductivities can change adaptively with objects in the vicinity, just like chameleons whose colors can change with nearby objects. Such an idea is, to some extent, inspired by natural creatures because they have helped scientific development from the aspects of phenomena and/or mechanisms, such as structure colors [16,17], adaptive camouflage [18,19], radiation cooling [20,21], and so on. In what follows, the scheme is validated by theory, simulation, and experiment.

II. THEORY FOR CHAMELEONLIKE THERMAL METASHELLS

The essence of chameleonlike thermal metashells is their adaptively changing thermal conductivities. Let us start by considering the two-dimensional system shown in Fig. 1(a). The system is split by the metashell (Region II) into three regions, whose tensorial conductivities are $\tilde{\kappa}_1$, $\tilde{\kappa}_2$, and $\tilde{\kappa}_3$, corresponding to Regions I, II, and III,

*jphuang@fudan.edu.cn

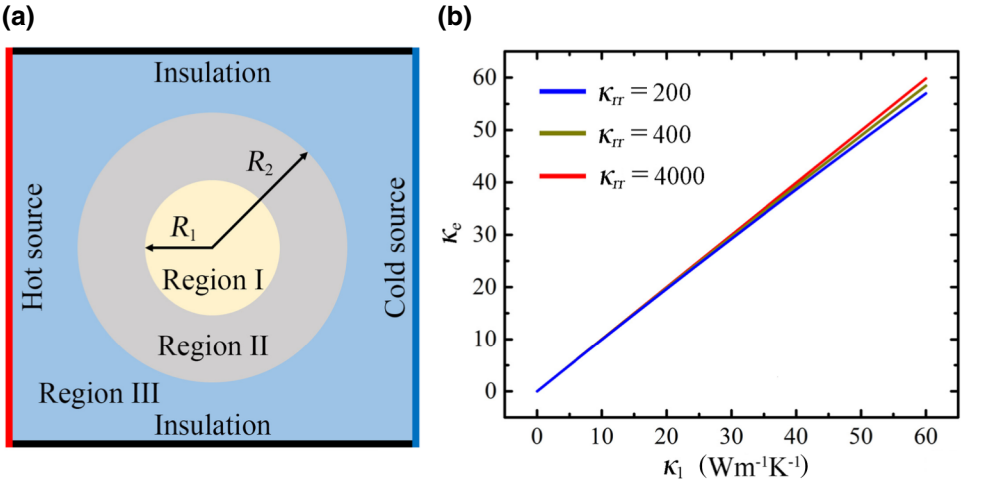

FIG. 1. Chameleonlike thermal metashells: (a) schematic graph; (b) the calculated overall thermal conductivity κ_e (Region I+II), as a function of κ_1 (Region I). The parameters are $R_1 = 4.8$ cm, $R_2 = 7.2$ cm, and $\kappa_{\theta\theta} = 0^+$ as required by Eq. (5).

respectively. Without loss of generality, we first suppose the object (Region I) and background (Region III) are isotropic, and the metashell (Region II) is anisotropic: $\tilde{\kappa}_1 = \kappa_1 \tilde{I}_2$, $\tilde{\kappa}_3 = \kappa_3 \tilde{I}_2$, and $\tilde{\kappa}_2 = \mathrm{diag}\,(\kappa_{rr}, \kappa_{\theta\theta})$. Here, $\tilde{I}_2$ is the second-order identity matrix, and all the tensors adopted in this work are expressed in cylindrical coordinates (r, θ) unless otherwise indicated. Then we can derive the overall thermal conductivity of Region I+II (denoted by κ_e) as

$$\kappa_e = m_1\kappa_{rr}\frac{\kappa_1 + m_1\kappa_{rr} + (\kappa_1 - m_1\kappa_{rr})\left(\sqrt{p}\right)^{2m_1}}{\kappa_1 + m_1\kappa_{rr} - (\kappa_1 - m_1\kappa_{rr})\left(\sqrt{p}\right)^{2m_1}}, \quad (1)$$

where $m_1 = \sqrt{\kappa_{\theta\theta}/\kappa_{rr}}$ and $p = (R_1/R_2)^2$ is the area fraction. A detailed derivation for obtaining Eq. (1) can be found in the Appendix.

Then, we calculate the limit of κ_e when $\kappa_{\theta\theta}/\kappa_{rr}$ goes to 0,

$$\kappa_e = \kappa_{rr}\frac{\kappa_1 - \kappa_{\theta\theta}\ln\sqrt{p}}{\kappa_{rr} - \kappa_1\ln\sqrt{p}}. \quad (2)$$

We resort to Eq. (2) to find out the requirement of chameleonlike metashells. As the name suggests, the chameleonlike metashell changes its thermal conductivity with nearby objects (located in Region I),

$$\kappa_2 = \kappa_1, \quad (3)$$

where κ_2 is the effective scalar thermal conductivity of the chameleonlike metashell (Region II). Since the thermal conductivity of Region I or II is κ_1, that (κ_e) of Region I+II has the only possibility to be

$$\kappa_e = \kappa_1. \quad (4)$$

Comparing Eq. (3) with Eq. (2), we obtain the requirement of the metashell as

$$\kappa_{\theta\theta} = 0^+ \text{ and } \kappa_{rr} \gg \kappa_1, \quad (5)$$

for $\kappa_{\theta\theta}/\kappa_{rr} \to 0$. Clearly, Eq. (5) makes Eq. (2) satisfy the requirement of Eq. (4). Here, $\kappa_{\theta\theta} = 0^+$ is a physical condition, which can be realized by materials with low thermal conductivities, such as air (with thermal conductivity 0.026 $\mathrm{W\,m^{-1}\,K^{-1}}$). Incidentally, a larger κ_{rr} could yield a better chameleonlike behavior as numerically demonstrated in Fig. 1(b).

III. FINITE-ELEMENT SIMULATIONS AND LABORATORY EXPERIMENTS OF CHAMELEONLIKE THERMAL METASHELLS

To validate the theory, we firstly perform finite-element simulations of the proposed chameleonlike metashells based on the commercial software COMSOL MULTIPHYSICS [22].

There are three regions in Figs. 2(a)–2(f) just like Fig. 1(a). Chameleonlike metashells, normal shells, and reference shells are, respectively, applied in Region II of Figs. 2(a) and 2(d), 2(b) and 2(e), and 2(c) and 2(f). For the convenience of comparison, we set the background (Region III) to have the same thermal conductivity as the corresponding object (Region I). Therefore, to check whether the thermal conductivity of the metashell (Region II) changes with the object inside (Region I), we can just compare the temperature profiles in the background (Region III) corresponding to the chameleonlike metashell and the reference shell. If the temperature profiles are the same, the proposed chameleonlike metashell does work as expected.

When the chameleonlike metashell reaches an object [Fig. 2(a)], it adaptively changes its thermal conductivity corresponding to the object, which results in the same temperature profile in the background (Region III) as the reference shell [Fig. 2(c)]. However, the normal shell distorts the background isotherms [Fig. 2(b)] due to its different thermal conductivity. Further, we change the thermal conductivity of the object, but keep the metashell unchanged [Fig. 2(d)]. As a result, the thermal conductivity of the

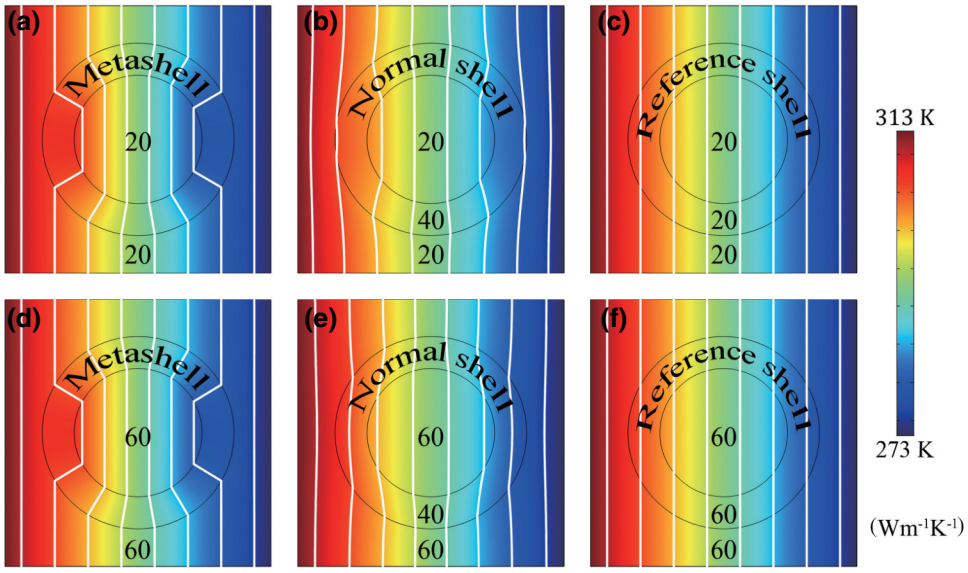

FIG. 2. Finite-element simulations of chameleonlike thermal metashells. The thermal conductivities of (a),(d) chameleonlike metashell and (b),(e) normal shell are diag(4000, 0) and 40 $\mathrm{W\,m^{-1}\,K^{-1}}$, respectively. The thermal conductivities of the object (Region I) and background (Region III) are set to be the same, which are (a)–(c) 20 and (d)–(f) 60 $\mathrm{W\,m^{-1}\,K^{-1}}$. The thermal conductivities of reference shells in (c),(f) are the same as those of corresponding objects. The simulation box in (a)–(f) is 20×20 $\mathrm{cm^2}$, $R_1 = 4.8$ cm, and $R_2 = 7.2$ cm. White lines represent isotherms.

chameleonlike metashell also adaptively changes, which results in the same background temperature profile as that corresponding to the reference shell [Fig. 2(f)]. In this case, the normal shell fails to change again [Fig. 2(e)]. The parameters of the chameleonlike metashell are designed according to Eq. (5) and the performance of Figs. 2(a) and 2(d) echoes the red line in Fig. 1(b).

For experimental validation, we set up the measuring device shown in Fig. 3(a). We further fabricate two experimental samples [Figs. 3(b) and 3(f)] to validate the simulations shown in Figs. 2(a) and 2(d). The parameters of the chameleonlike metashell in Figs. 2(a) and 2(d) are very ideal, but here we use approximate parameters to conduct experiments without affecting the results. The two samples are fabricated by laser cutting and measured by the apparatus shown in Fig. 3(a). The corresponding measured results are shown in Figs. 3(c) and 3(g), which prove that the thermal conductivity of the chameleonlike metashell does change with different objects. We also perform simulations based on the two samples to remove the effects of convection and radiation, which are shown in Figs. 3(d) and 3(h). As references, Figs. 3(e) and 3(i) show the simulation results of the pure background with drilled air holes whose sizes are the same as the background in Figs. 3(b) and 3(f). Both simulations [Figs. 2(a) and 2(d) and Figs. 3(d) and 3(h)] and experiments [Figs. 3(c) and 3(g)] help to validate the feasibility of the chameleonlike metashell. In addition, we also calculate the effective thermal conductivity

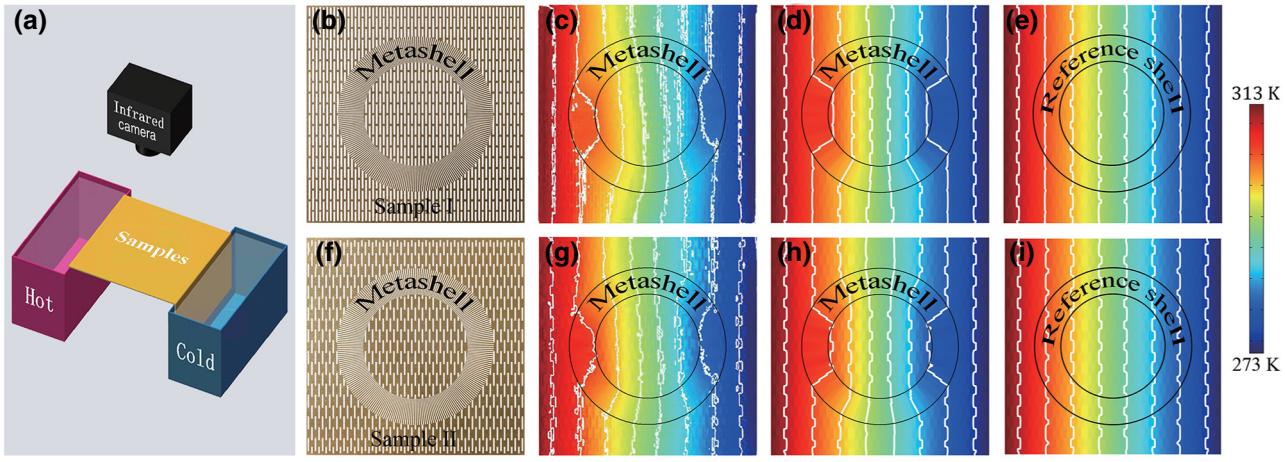

FIG. 3. Laboratory experiments of chameleonlike thermal metashells. (a) Experimental setup. (b),(f) Photos of two samples. The measured and simulation results of (b) [or (f)] are shown in (c),(g) [or (d),(h)], respectively. (e),(i) Simulation results of the pure background as adopted in (b),(f), respectively. The thermal conductivities of the copper and air are 400 and 0.026 $\mathrm{W\,m^{-1}\,K^{-1}}$, respectively. These parameters cause the tensorial thermal conductivity of the chameleonlike metashell in (b),(f) to be diag (264.68, 0.08) $\mathrm{W\,m^{-1}\,K^{-1}}$ and the thermal conductivities of the object [or background] to be 20 $\mathrm{W\,m^{-1}\,K^{-1}}$ for (b) and 60 $\mathrm{W\,m^{-1}\,K^{-1}}$ for (f). The sample sizes in (b),(f) are the same as those for Fig. 2(a).

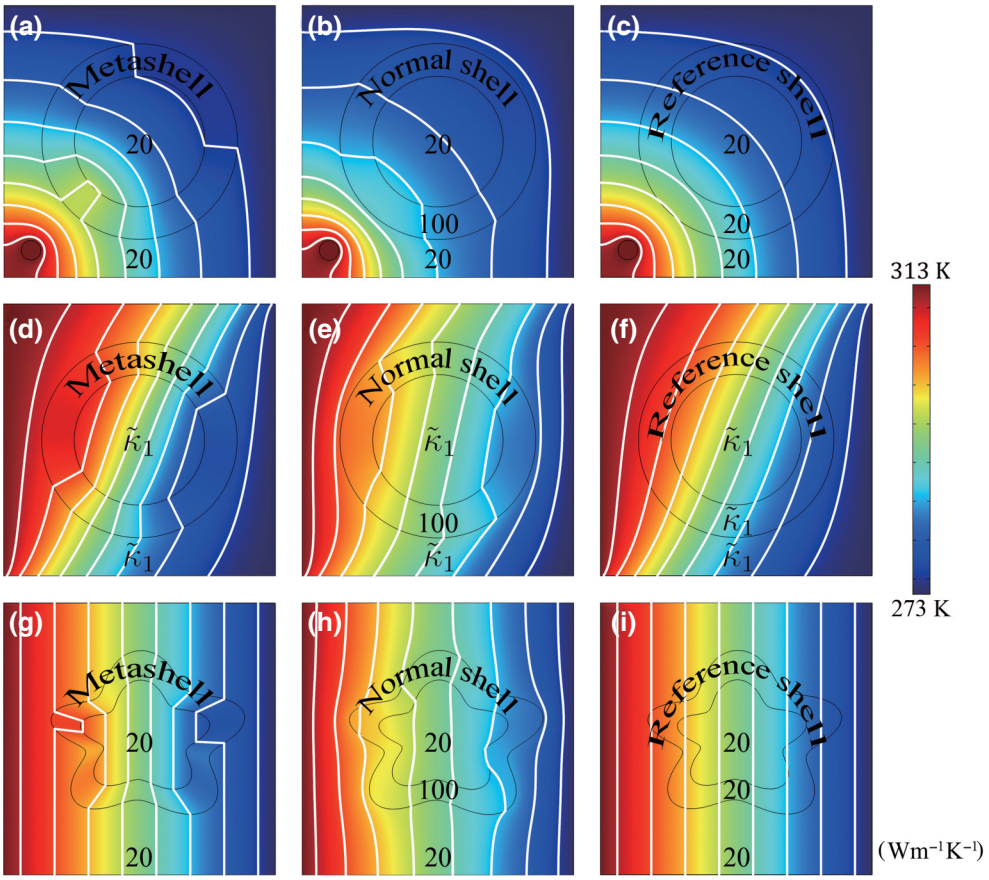

FIG. 4. Finite-element simulations of extended chameleonlike thermal metashells: (a)–(c) nonuniform fields generated by point heat sources; (d)–(f) anisotropic objects; (g)–(i) noncircular shapes. The thermal conductivities of object/background are (a)–(c) and (g)–(i) 20 $\mathrm{W\,m^{-1}\,K^{-1}}$ and (d)–(f) $[(30, 20), (20, 30)]$ $\mathrm{W\,m^{-1}\,K^{-1}}$ (tensorial form in Cartesian coordinates). The metashell in (a), (d), and (g) is the same as that in Figs. 2(a) and 2(d), namely, $\mathrm{diag}(4000, 0)$ $\mathrm{W\,m^{-1}\,K^{-1}}$. The thermal conductivity of the normal shell is 100 $\mathrm{W\,m^{-1}\,K^{-1}}$. The thermal conductivity of the reference shell is the same as that of the corresponding object, namely 20 $\mathrm{W\,m^{-1}\,K^{-1}}$ for (c),(i), and $[(30, 20), (20, 30)]$ $\mathrm{W\,m^{-1}\,K^{-1}}$ for (f). Other parameters are the same as those for Fig. 2(a).

changing with different structure parameters to ensure the completeness of our experiment; see Fig. 5 in the Appendix.

Finally, we extend the chameleonlike metashell from uniform to nonuniform fields, from isotropic to anisotropic objects, and from circular to complex shapes; see Fig. 4. Chameleonlike metashells, normal shells, and reference shells are applied in Figs. 4(a), 4(d), and 4(g); Figs. 4(b), 4(e), and 4(h); and Figs. 4(c), 4(f), and 4(i), respectively. When the chameleonlike metashell reaches an object with nonuniform fields [Fig. 4(a)], it adaptively changes its thermal conductivity corresponding to the object, which results in the same temperature profile in the background (Region III) as the reference shell [Fig. 4(c)]. However, the normal shell distorts the background isotherms [Fig. 4(b)] significantly due to its different thermal conductivity. Similarly, when the chameleonlike metashell reaches an object with anisotropic parameters [Fig. 4(d)], it adaptively changes its thermal conductivity corresponding to the anisotropic object, which results in the same temperature profile in the background (Region III) as the reference shell [Fig. 4(f)]. However, the normal shell also distorts the background isotherms [Fig. 4(e)] due to its different thermal conductivity. Then, we arbitrarily change the shape of the chameleonlike metashell (without changing the other parameters) to check whether it still works. The same temperature profile in background (Region III) between Figs. 4(g) and 4(i) demonstrates the ability of the chameleonlike shell. Again, the normal shell distorts the background isotherms [Fig. 4(h)]. These results show that our chameleonlike metashells are robust under different conditions.

IV. DISCUSSION AND CONCLUSION

By developing a theory, we reveal a type of counterintuitive chameleonlike behavior in thermal conduction: the joint thermal effect of a metashell (Region II with radius between R_1 and R_2) and object (Region I with radius R_1) on a background (Region III) is always the same as the thermal effect of the pure object (with radius R_2) on the same background, while the object changes with different conductivities and/or temperature distributions. Namely, in this case, the metashell (Region II) always adapts to the changing objects (Region I) well; thus, we call it chameleonlike behavior. This behavior predicted by our theory is further confirmed by finite-element simulations and laboratory experiments.

The proposed chameleonlike meteshells can work as a type of all-purpose material to meet different requirements of thermal conductivities under different conditions. For example, thermal conductivities are expected to be

relatively low in a thermal protection field, whereas they are expected to be relatively high in a thermal dissipation field. Chameleonlike meteshells may address these problems owing to their adaptive thermal conductivities.

The present chameleonlike metashells are well behaved in steady states since we do not consider the effects of both densities and heat capacities. Certainly, chameleonlike metashells in transient states are promising as well and good results can be expected in light of the pioneering results on transient states [3,5,23,24].

In summary, the passive chameleonlike metashells proposed in this work require no preknowledge (namely, thermal conductivities and temperature distributions) of nearby objects, but can work adaptively for different adjacent objects. Such metashells can act as a type of all-purpose material and have potential applications in novel camouflaging, self-adaption, etc. Our work suggests a passive method for achieving intelligent thermal metamaterials in sharp contrast to the existing active methods and also offers hints on how to design similar behaviors in electrostatics, magnetostatics, and particle diffusion (where electric conductivities, magnetic permeabilities, and diffusion constants, respectively, play the same role as thermal conductivities in thermotics).

ACKNOWLEDGMENTS

We acknowledge the financial support by the National Natural Science Foundation of China under Grant No. 11725521.

APPENDIX

1. Details for deriving Eq. (1)

Let us consider the governing equation of heat conduction,

$$\nabla \cdot (-\tilde{\kappa} \nabla T) = 0, \tag{A1}$$

where $\tilde{\kappa}$ and T are tensorial thermal conductivity and temperature, respectively.

Equation (A1) in Region II can be expanded in cylindrical coordinates (r, θ) as

$$\frac{1}{r}\frac{\partial}{\partial r}\left(r\kappa_{rr}\frac{\partial T_2}{\partial r}\right) + \frac{1}{r}\frac{\partial}{\partial \theta}\left(\kappa_{\theta\theta}\frac{\partial T_2}{r\partial \theta}\right) = 0, \tag{A2}$$

where T_2 is the temperature in Region II. By analogy, T_1 and T_3 can be defined for Region I and Region III.

The general solution of Eq. (A2) is

$$T_2 = A_0 + B_0 \ln r + \sum_{i=1}^{\infty} \left[A_i \sin(i\theta) + B_i \cos(i\theta)\right] r^{im_1} + \sum_{j=1}^{\infty} \left[C_j \sin(j\theta) + D_j \cos(j\theta)\right] r^{jm_2}, \tag{A3}$$

where $m_{1,2} = \pm\sqrt{\kappa_{\theta\theta}/\kappa_{rr}}$. T_1 and T_3 can also be given by the right side of Eq. (A3) with $m_{1,2} = \pm 1$. The coefficients in T_1, T_2, and T_3 can be determined by the following boundary conditions:

$$\begin{cases} T_1 < \infty, \\ T_1(R_1) = T_2(R_1), \\ T_2(R_2) = T_3(R_2), \\ (-\kappa_1 \partial T_1/\partial r)_{R_1} = (-\kappa_{rr}\partial T_2/\partial r)_{R_1}, \\ (-\kappa_{rr}\partial T_2/\partial r)_{R_2} = (-\kappa_3 \partial T_3/\partial r)_{R_2}, \\ \nabla T_3 (r \to \infty) = \nabla T_0, \end{cases} \tag{A4}$$

where ∇T_0 represents the external uniform temperature gradient.

Considering the symmetry of boundary conditions, we only need to keep several terms of Eq. (A3) to calculate T_1, T_2, and T_3, say

$$T_1 = A_0 + B_{11} r \cos\theta, \tag{A5}$$

$$T_2 = A_0 + B_{12} r^{m_1} \cos\theta + D_{12} r^{m_2} \cos\theta, \tag{A6}$$

$$T_3 = A_0 + B_{13} r \cos\theta + D_{13} r^{-1} \cos\theta, \tag{A7}$$

where the temperature at $\theta = \pm\pi/2$ is defined as A_0.

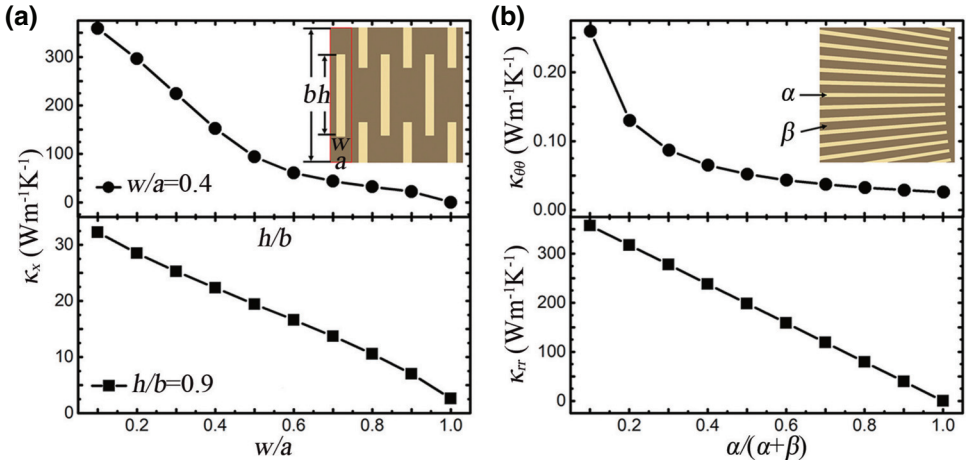

FIG. 5. Microstructure effects on effective thermal conductivities of (a) the background and (b) the chameleonlike metashell. The dark area is copper with thermal conductivity 400 $\mathrm{W\,m^{-1}\,K^{-1}}$, and light area is air with thermal conductivity 0.026 $\mathrm{W\,m^{-1}\,K^{-1}}$. Other parameters are $b/a = 6.1$ for (a) and $\alpha = 0.5$ degrees for (b).

With Eqs. (A5)–(A7), Eq. (A4) can then be simplified as

$$\begin{cases} B_{11}R_1 = B_{12}R_1^{m_1} + D_{12}R_1^{m_2}, \\ B_{12}R_2^{m_1} + D_{12}R_2^{m_2} = B_{13}R_2 + D_{13}R_2^{-1}, \\ \kappa_1 B_{11} = \kappa_{rr}\left(m_1 B_{12}R_1^{m_1-1} + m_2 D_{12}R_1^{m_2-1}\right), \\ \kappa_{rr}\left(m_1 B_{12}R_2^{m_1-1} + m_2 D_{12}R_2^{m_2-1}\right) = \kappa_3\left(B_{13} - D_{13}R_2^{-2}\right), \\ B_{13} = |\nabla T_0|\,. \end{cases} \tag{A8}$$

Solving Eq. (A8), we can derive

$$\begin{cases} B_{11} = \dfrac{-4R_1^{m_1-1}R_2^{m_1+1}m_1\kappa_{rr}\kappa_3\,|\nabla T_0|}{R_1^{2m_1}\left(-\kappa_1 + m_1\kappa_{rr}\right)\left(m_1\kappa_{rr} - \kappa_3\right) - R_2^{2m_1}\left(\kappa_1 + m_1\kappa_{rr}\right)\left(m_1\kappa_{rr} + \kappa_3\right)}, \\ B_{12} = \dfrac{2\left(\kappa_1 + m_1\kappa_{rr}\right)R_2^{m_1+1}\kappa_3\,|\nabla T_0|}{R_1^{2m_1}\left(\kappa_1 - m_1\kappa_{rr}\right)\left(m_1\kappa_{rr} - \kappa_3\right) + R_2^{2m_1}\left(\kappa_1 + m_1\kappa_{rr}\right)\left(m_1\kappa_{rr} + \kappa_3\right)}, \\ D_{12} = \dfrac{-2(\kappa_1 - m_1\kappa_{rr})R_1^{2m_1}R_2^{m_1+1}\kappa_3|\nabla T_0|}{R_1^{2m_1}(\kappa_1 - m_1\kappa_{rr})(m_1\kappa_{rr} - \kappa_3) + R_2^{2m_1}(\kappa_1 + m_1\kappa_{rr})(m_1\kappa_{rr} + \kappa_3)}, \\ B_{13} = |\nabla T_0|\,, \\ D_{13} = \dfrac{R_1^{2m_1}\left(-\kappa_1 + m_1\kappa_{rr}\right)\left(m_1\kappa_{rr} + \kappa_3\right) - R_2^{2m_1}\left(\kappa_1 + m_1\kappa_{rr}\right)\left(m_1\kappa_{rr} - \kappa_3\right)}{R_1^{2m_1}\left(\kappa_1 - m_1\kappa_{rr}\right)\left(m_1\kappa_{rr} - \kappa_3\right) + R_2^{2m_1}\left(\kappa_1 + m_1\kappa_{rr}\right)\left(m_1\kappa_{rr} + \kappa_3\right)}R_2^2\,|\nabla T_0|\,, \end{cases} \tag{A9}$$

where m_2 disappears because we replace m_2 with $-m_1$ for brevity.

Finally, we set D_{13} to be zero, thus ensuring the thermal field of the background to be uniform. Then we can derive the value of κ_3, which is exactly the overall thermal conductivity of Region I+II (denoted by κ_e) as shown in Eq. (1).

2. Details for laboratory experiments

To realize the thermal conductivity of the background (20 and 60 $\mathrm{W\,m^{-1}\,K^{-1}}$), we drill different rectangular air holes on a copper plate. The effective thermal conductivities of the drilled coppers corresponding to different rectangle sizes are obtained from finite-element simulations. The upper and lower figures in Fig. 5(a) show the effects on changing the rectangle height and width, respectively. To realize the thermal conductivity of 20 $\mathrm{W\,m^{-1}\,K^{-1}}$, we set $a = 0.328$, $b = 2$, $w = 0.164$, and $h = 1.8$ cm. To realize the thermal conductivity of 60 $\mathrm{W\,m^{-1}\,K^{-1}}$, we set $a = 0.328$, $b = 2$, $w = 0.131$, and $h = 1.2$ cm.

To realize the required thermal conductivity of the chameleonlike metashell, we design the layer structure presented in Fig. 5(b). The upper and lower figures in Fig. 5(b) demonstrate the tangential thermal conductivity and radial thermal conductivity, respectively. We set $\alpha = 0.5$ and $\beta = 1$ degree to fabricate the two samples.

Then, we use the infrared camera Flir E60 to measure the temperature distributions. To reduce the infrared reflection and thermal convection, we use transparent plastic and foamed plastic (both insulated) to cover the upper and lower surfaces, respectively.

[1] C. Z. Fan, Y. Gao, and J. P. Huang, Shaped graded materials with an apparent negative thermal conductivity, Appl. Phys. Lett. **92**, 251907 (2008).

[2] T. Y. Chen, C.-N. Weng, and J.-S. Chen, Cloak for curvilinearly anisotropic media in conduction, Appl. Phys. Lett. **93**, 114103 (2008).

[3] S. Guenneau, C. Amra, and D. Veynante, Transformation thermodynamics: Cloaking and concentrating heat flux, Opt. Express **20**, 8207 (2012).

[4] S. Narayana and Y. Sato, Heat Flux Manipulation with Engineered Thermal Materials, Phys. Rev. Lett. **108**, 214303 (2012).

[5] R. Schittny, M. Kadic, S. Guenneau, and M. Wegener, Experiments on Transformation Thermodynamics: Molding the Flow of Heat, Phys. Rev. Lett. **110**, 195901 (2013).

[6] H. Y. Xu, X. H. Shi, F. Gao, H. D. Sun, and B. L. Zhang, Ultrathin Three-Dimensional Thermal Cloak, Phys. Rev. Lett. **112**, 054301 (2014).

[7] T. C. Han, X. Bai, D. L. Gao, J. T. L. Thong, B. W. Li, and C.-W. Qiu, Experimental Demonstration of a Bilayer Thermal Cloak, Phys. Rev. Lett. **112**, 054302 (2014).

[8] Y. G. Ma, Y. C. Liu, M. Raza, Y. D. Wang, and S. L. He, Experimental Demonstration of a Multiphysics Cloak: Manipulating Heat Flux and Electric Current Simultaneously, Phys. Rev. Lett. **113**, 205501 (2014).

[9] Q. Ma, Z. L. Mei, S. K. Zhu, T. Y. Jin, and T. J. Cui, Experiments on Active Cloaking and Illusion for Laplace Equation, Phys. Rev. Lett. **111**, 173901 (2013).
[10] D. M. Nguyen, H. Y. Xu, Y. M. Zhang, and B. L. Zhang, Active thermal cloak, Appl. Phys. Lett. **23**, 016623 (2015).
[11] C. W. Lan, K. Bi, Z. H. Gao, B. Li, and J. Zhou, Achieving bifunctional cloak via combination of passive and active schemes, Appl. Phys. Lett. **109**, 1777 (2016).
[12] Y. Li, X. Y. Shen, Z. H. Wu, J. Y. Huang, Y. X. Chen, Y. S. Ni, J. P. Huang, Temperature-dependent transformation thermotics, From Switchable Thermal Cloaks to Macroscopic Thermal Diodes, Phys. Rev. Lett. **115**, 195503 (2015).
[13] X. Y. Shen, Y. Li, C. R. Jiang, and J. P. Huang, Temperature Trapping: Energy-Independent Maintenance of Constant Temperatures as Ambient Temperature Gradients Change, Phys. Rev. Lett. **117**, 055501 (2016).
[14] X. Y. Shen, Y. Li, C. R. Jiang, Y. S. Ni, and J. P. Huang, Thermal cloak-concentrator, Appl. Phys. Lett. **109**, 031907 (2016).
[15] R. G. Peng, Z. Q. Xiao, Q. Zhao, F. L. Zhang, Y. G. Meng, B. Li, J. Zhou, Y. C. Fan, P. Zhang, N.-H. Shen, T. Koschny, and C. M. Soukoulis, Temperature-Controlled Chameleonlike Cloak, Phys. Rev. X **7**, 011033 (2017).
[16] J. Zi, X. D. Yu, Y. Z. Li, X. H. Hu, C. Xu, X. J. Wang, X. H. Liu, and R. T. Fu, Coloration strategies in peacock feathers, Proc. Natl. Acad. Sci. USA **100**, 12576 (2003).
[17] Y. F. Zhang, B. Q. Dong, A. Chen, X. Shi, L. Shi, and J. Zi, Using cuttlefish ink as an additive to produce non-iridescent structural colors of high color visibility, Adv. Mater. **27**, 4719 (2015).
[18] V. S. Ramachandran, C. W. Tyler, R. L. Gregory, D. Rogers-Ramachandran, S. Duensing, C. Pillsbury, and C. Ramachandran, Rapid adaptive camouflage in tropical flounders, Nature **379**, 815 (1996).
[19] C. J. Yu, Y. H. Li, X. Zhang, X. Huang, V. Malyarchuk, S. D. Wang, Y. Shi, L. Gao, Y. W. Su, Y. H. Zhang, H. X. Xu, R. T. Hanlon, Y. G. Huang, and J. A. Rogers, Adaptive optoelectronic camouflage systems with designs inspired by cephalopod skins, Proc. Natl. Acad. Sci. USA **111**, 12998 (2014).
[20] N. N. Shi, C.-C. Tsai, F. Camino, G. D. Bernard, N. F. Yu, and R. Wehner, Keeping cool: Enhanced optical reflection and radiative heat dissipation in Saharan silver ants, Science **349**, 298 (2015).
[21] Y. Zhai, Y. G. Ma, S. N. David, D. L. Zhao, R. N. Lou, G. Tan, R. G. Yang, and X. B. Yin, Scalable-manufactured randomized glass-polymer hybrid metamaterial for daytime radiative cooling, Science **355**, 1062 (2017).
[22] http://www.comsol.com/.
[23] S. R. Sklan, X. Bai, B. W. Li, and X. Zhang, Detecting thermal cloaks via transient effects, Sci. Rep. **6**, 32915 (2016).
[24] T. Z. Yang, Y. Su, W. Xu, and X. D. Yang, Transient thermal camouflage and heat signature control, Appl. Phys. Lett. **109**, 121905 (2016).